Lab on a Chip

Accepted Manuscript

Lab on a Chip

Volume 1 | Number 1 | Jan 2013 | Pages 1–100

Miniaturisation for chemistry, physics, biology, materials science and bioengineering
www.rsc.org/loc

ROYAL SOCIETY OF CHEMISTRY

This is an *Accepted Manuscript*, which has been through the Royal Society of Chemistry peer review process and has been accepted for publication.

Accepted Manuscripts are published online shortly after acceptance, before technical editing, formatting and proof reading. Using this free service, authors can make their results available to the community, in citable form, before we publish the edited article. We will replace this *Accepted Manuscript* with the edited and formatted *Advance Article* as soon as it is available.

You can find more information about *Accepted Manuscripts* in the **Information for Authors**.

Please note that technical editing may introduce minor changes to the text and/or graphics, which may alter content. The journal's standard **Terms & Conditions** and the **Ethical guidelines** still apply. In no event shall the Royal Society of Chemistry be held responsible for any errors or omissions in this *Accepted Manuscript* or any consequences arising from the use of any information it contains.

ROYAL SOCIETY OF CHEMISTRY

www.rsc.org/loc

ARTICLE TYPE

Characterisation of oxygen permeation into a microfluidic device for cell culture by in-situ NMR spectroscopy

Ali Yilmaz[*a] and Marcel Utz,[a]

A compact microfludic device for perfusion culture of mammalian cells under in-situ metabolomic observation by NMR spectroscopy is presented. The chip is made from poly(methyl methacrylate) (PMMA), and uses a poly(dimethyl siloxane) (PDMS) membrane to allow gas exchange. It is integrated with a generic micro-NMR detector developed recently in our group [*J. Magn. Reson.* **262**, 73–80 (2016)]. While PMMA is an excellent material in the context of NMR, PDMS is known to produce strong background signals. To mitigate this, the device keeps the PDMS away from the detection area.

The oxygen permeation into the device is quantified using a flow chemistry approach. A solution of glucose is mixed on the chip with one of glucose oxidase, before flowing through the gas exchanger. The resulting concentration of gluconate is measured by ^{1}H NMR spectroscopy as a function of flow rate. An oxygen equilibration rate constant of 2.4 s^{-1} is found for the device, easily sufficient to maintain normoxic conditions in a cell culture at modest perfusion flow rates.
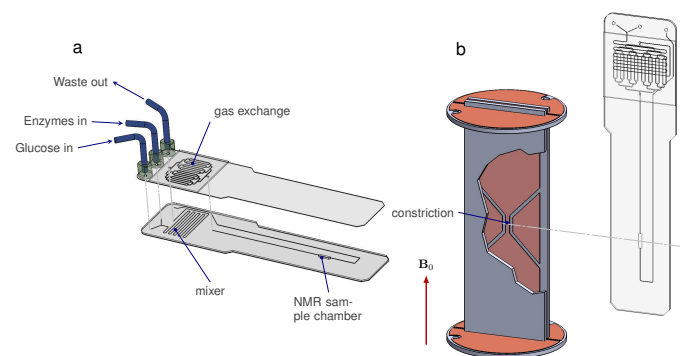
Fig. 1 Transmission line NMR detector[1] and gas exchange chip. The chip is composed of three layers of PMMA (right). Glucose and enzyme solutions are injected into the mixer on the middle layer, and are then transported through a via up into the gas exchange channels engraved into the top layer, which are covered by a PDMS membrane.

1 INTRODUCTION

NMR spectroscopy is a highly useful tool to study the metabolic manifold (metabolome) in live systems. NMR can provide quantitative information on hundreds of metabolites non-invasively, without requiring any sample preparation. It can be used directly on live systems to monitor biochemical activity.

Microfluidic culture of cells[2] and tissue slices[3] holds great promise for medical diagnostics, drug development, and drug safety testing, among other life science applications, providing an alternative to animal testing. Microfabricated structures allow very precise control of the extracellular microenvironment, including the interaction with other cells, extracellular matrix, soluble factors, and mechanical forces[4]. Also, analytical biosensors can be integrated directly into the culture platform, thus combining living cells and sensors for detection of cellular physiological parameters and analysis of external stimuli in situ[5].

Our long-term objective is to develop a microfluidic platform for cell culture that can be directly inserted into a conventional NMR spectrometer for metabolomic monitoring. As an important step towards this goal, the present paper reports a microfluidic chip that combines the ability to exchange oxygen with the environment with high-resolution and high-sensitivity ^{1}H NMR spectroscopy.

Gas exchange in microfluidic culture devices is usually ensured either by leaving the culture chamber open to the atmosphere (similar to well plates), or by exploiting the excellent gas permeability of poly(dimethyl siloxane) (PDMS)[6]. While leaving the chip open is not acceptable in our application since the chip must be transferred between the incubator and the NMR spectrometer without contamination, PDMS is a problematic material in the context of NMR spectroscopy due to the large background signals arising from its methyl groups.

To solve this problem, we have designed a PMMA device that spatially separates the gas exchange with the environment through a PDMS membrane from the NMR sampling area. The chip is compatible with a high-performance transmission line NMR probe that has recently been developed in our group[1]. In contrast to PDMS, which is a liquid on NMR time scales, PMMA is a glassy solid. Its protons therefore experience large mutual dipolar couplings, which lead to a very broad NMR signal, which is easily distinguished from the desired signal from the sample fluid by its short decay time (typically well within the receiver dead time).

[a] *School of Chemistry, University of Southampton, United Kingdom SO17 1BJ.*

NMR spectroscopy is widely used in the metabolomic characterisation of live systems. Due to the limited sensitivity, this has been restricted mainly to monitoring of large organisms (e.g., humans) by way of body fluids readily available in large quantities[7]. However, significant progress in miniaturising NMR detectors has enabled integration of NMR spectroscopy and microfluidics[8-16]. Recently, some metabolomic NMR studies at the microfluidic scale have been reported[17,18].

Several groups have reported integration of simple microfluidic chips, consisting of a sample chamber and fluidic access points, with micro-NMR detectors[1,13,15]. However, unlocking the real power of microfluidic NMR requires integrating chips with more complex functionality with sensitive NMR detectors[19]. Our aim is to take this a step further, demonstrating the integration of a functional culture chip capable of gas exchange, cell culture, and perfusion, with NMR spectroscopy.

In this contribution, we describe a hybrid microfluidic device made from PMMA and PDMS that is suitable for microfluidic perfusion cell culture, and can be inserted into a conventional NMR spectrometer for high-resolution spectroscopy (cf. Fig. 1). The PDMS allows gas exchange with the environment. The main aim of the work reported in the following was to (a) develop a reliable fabrication protocol for this device, and (b) to quantify the rate of oxygen exchange in it by NMR spectroscopy.

2 THEORY AND DESIGN

The device used in this study is shown in Fig. 1. It is fabricated from three layers of PMMA (back layer, middle layer, and cover layer), and a layer of PDMS. Two inlets feed into a serpentine mixer, which is connected to a set of 16 parallel gas exchange channels through a hierarchy of binary dividers. The gas exchange channels are covered by the PDMS layer; gas exchange with the ambient atmosphere happens by diffusion between the fluid channels and the surface of the PDMS layer. The fluid is then guided into the sample chamber. The fluidic features are arranged in two planes; the mixer, most of the connecting channels, and the sample chamber are cut into the middle layer, while the gas exchange channels are cut into the top of the cover layer. Cylindrical vias of 0.5 mm diameter provide fluidic connections between the layers.

The double inlets and the mixer are part of the design specifically in order to characterise the oxygen exchange, and are not needed for perfusion culture. In this case, a variant of the chip will be used with a single inlet and outlet, to be interfaced with a piezoelectric micro pump that circulates the culture medium through the chip.

The kinetics of oxygen uptake through the gas exchanger have been quantified by feeding buffered solutions of (i) glucose, and (ii) glucose oxidase / horseradish peroxidase into the two inlets at defined flow rates using syringe pumps, as described in the experimental section. The concentrations of glucose and the enzymes have been chosen such as to ensure that the reaction kinetics are only limited by the available oxy-
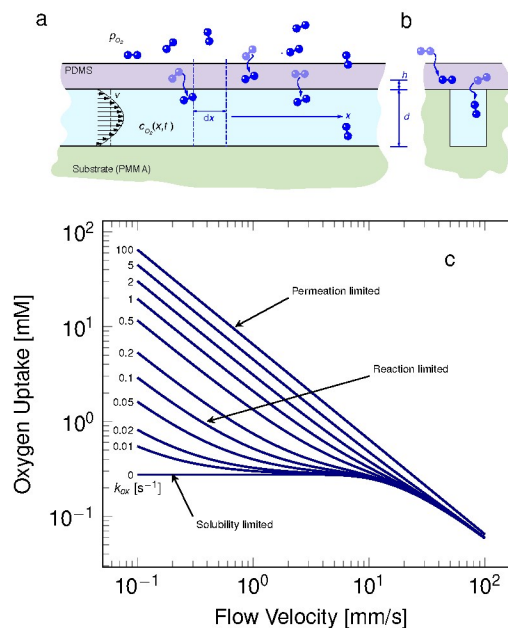

Fig. 2 Longitudinal (a) and axial (b) cross-section of a fluid-filled channel covered by an oxygen-permeable PDMS mebrane. (c) Theoretical total oxygen uptake by a glucose/glucose oxidase solution flowing through a channel of 0.1 mm depth, covered by a PDMS membrane of 0.2 mm thickness, as a function of flow velocity, for different values of the oxidation rate constant k_{ox}.

gen.

The resulting composition was then determined off-line by NMR spectroscopy. Gluconate gives peaks in the ^{1}H NMR spectrum that are well separated from the glucose background, which facilitates quantification of the amount of gluconate formed by integration.

The permeation of a gas through a polymer membrane can be described in terms of Fick's law as a flux proportional to the difference in partial pressure between the two sides:

$$ j = -\Pi \frac{p_2 - p_1}{h}, \tag{1} $$

where Π denotes the permeation coefficient, h is the membrane thickness, and j denotes the flux in units of Moles per square meter and second. An idealised geometry of an oxygen exchange channel is shown in Fig. 2. The solution enters from the left, with a flow velocity v, and exits on the right. The oxygen permeable PDMS membrane separates the fluid from an atmosphere with oxygen partial pressure p_{O_2}. Under laminar conditions, the flow velocity will exhibit a parabolic profile over the depth d of the channel, as indicated in the figure. We assume that the fluid entering from the left contains reagents (i.e., glucose and glucose oxidase) that consume oxygen. In the limit of high reagent and enzyme concentrations, this reaction is expected to follow pseudo first order kinetics, with a rate constant k_{ox}. While the full coupled transport/chemical reaction system exhibits considerable complexity due to the coupled permeation, diffusion, convection, and reaction pro-

cesses, we can make some assumptions for the present purpose that greatly simplify its treatment.

First, we assume diffusion of reagents and oxygen over the channel depth to be fast compared to all other processes. This allows us to replace the parabolic velocity profile with an average velocity v, as indicated by a dash-dotted line in the figure. Moreover, we can treat the oxygen concentration c as constant over the depth of the channel, with the only variations occurring in the x direction.

Around ambient pressure, the equilibrium concentration of oxygen in water in contact with an atmosphere with oxygen partial pressure p_{O_2} follows Henry's law

$$c_{eq} = k_H p_{O_2}. \qquad (2)$$

At our experimental temperature of $21°C$, the value of k_H is $k_H = 1.37 \, \mathrm{mM\,atm^{-1}};^{20}$ a 20% oxygen atmosphere at 1 atm pressure will then lead to concentration of dissolved molecular oxygen of $273 \, \mu$M.

The oxygen mass balance in a small volume element of length dx yields the continuity equation

$$\frac{\partial c}{\partial t} = -v\frac{\partial c}{\partial x} + \frac{\Pi}{hd}\left(p_{O_2} - \frac{c}{k_H}\right) - k_{ox}c. \qquad (3)$$

Under steady-state conditions, the time derivative vanishes, and we obtain the ODE

$$v\frac{dc}{dx} - (k_p + k_{ox})c - k_p c_{eq} = 0, \qquad (4)$$

where $k_p = \Pi/(hk_H d)$ is the permeation rate constant.

This equation can be solved analytically for the concentration profile $c(x)$. In the present context, however, we are interested to quantify the total amount of molecular oxygen transferred through the membrane into the streaming fluid. This can be computed from the steady-state concentration profile $c(x)$ by replacing x with vt, and integrating from $t = 0$ to $t = L/v$, where L is the length of the channel. Assuming the fluid enters the channel at $c = 0$, the total uptake per volume of fluid is thus found as

$$C = \frac{c_{eq}k_p^2}{(k_{ox}+k_p)^2}\left(1 - e^{-\frac{L(k_{ox}+k_p)}{v}} + \frac{k_{ox}}{k_p}\frac{L(k_{ox}+k_p)}{v}\right). \qquad (5)$$

This expression is plotted in Fig. 2. Depending on the relative magnitudes of k_{ox}, k_p, and v/L, three different regimes can be distinguished. At high velocities, when $v/L \gg k_p$, the uptake is limited by the amount of time the fluid spends exposed to the oxygen-permeable membrane in the channel. In this regime, the uptake is inversely proportional to the velocity.

For $k_{ox} \ll k_p$, this reduces to

$$C \approx c_{eq}\left(1 - e^{-\frac{Lk_p}{v}} + \frac{k_{ox}L}{v}\right). \qquad (6)$$

Obviously, if a channel is operated in this regime at low velocities ($v < Lk_p$), then the oxygen consumed by the reaction is continually replenished by permation through the membrane,
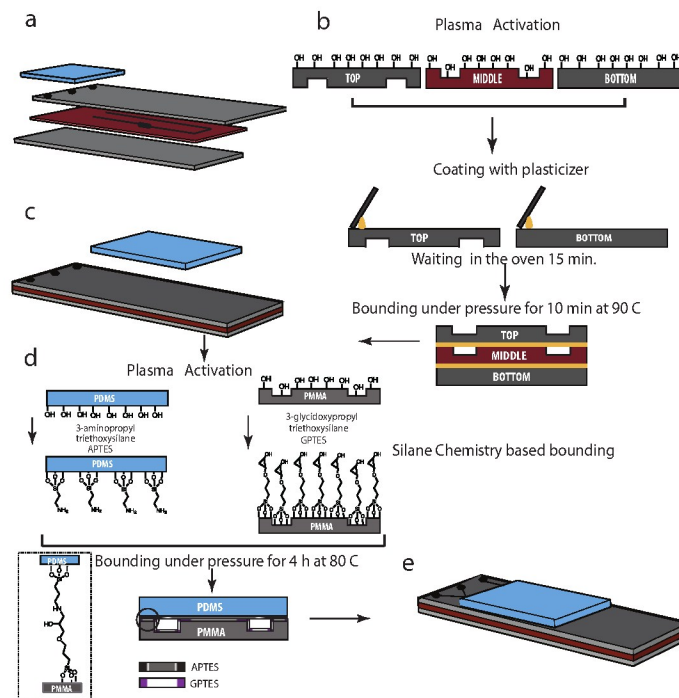

Fig. 3 Schematic of bonding process: a: PMMA and PDMS layers used for chip manufacturing; b: The surface modifications(plasma treatment and plasticizer coating) for bonding of PMMA pairs followed by hot-press bonding; c:microchip ready to bonding with PDMS membrane; d: Surface treatment followed by silane chemistry based bonding and hot-press bonding; e: finished chip ready for in-situ NMR experiment.

and the oxygen concentration remains near the saturation concentration c_{eq}. The total oxygen uptake is then controlled mainly by the residence time $t = L/v$ and the oxygen reaction constant k_{ox}. If $k_{ox} \gg k_p$, we obtain

$$C \approx c_{eq}\left(\frac{k_p^2}{k_{ox}^2} - \frac{k_p^2}{k_{ox}^2}e^{-\frac{Lk_{ox}}{v}} + \frac{k_pL}{v}\right). \qquad (7)$$

In this expression, the last term obviously dominates at very low velocities, whereas at high velocities, the first two terms tend to cancel out. Therefore, to a good approximation we can write

$$C \approx c_{eq}\frac{k_pL}{v} \qquad (8)$$

over the entire range of velocities.

3 MATERIALS AND METHODS

3.1 Chemicals and materials

Poly (methyl methacrylate) (PMMA) sheets (Clarex Precision sheets 0.5 mm and 0.2 mm, respectively) were purchased from Weatherall Equipment& Instruments Ltd. Poly (dimethylsiloxane) (PDMS) prepolymer (Sylgard 184) and a curing agent was purchased from Dow Corning (Midland,

MI, USA). 3-Aminopropyltriethoxysilane (APTES, 99%), dibutyl phthalate (DBP), 3-Glycid-oxypropyltriethoxysilane (GPTES), isopropanol,glucose oxidase, hydrogen peroxidase and ethanol were purchased from Sigma Aldrich. Aqueous solutions were prepared using deionized (DI) water. Solutions of glucose for NMR was diluted from a 1 M stock solution (from solid, >99.5%) prepared at least 24 hours before the experiments and stored at 4°C.

3.2 Microchannel fabrication

Device layouts were designed on AutoCAD. Microfluidic LoC devices were manufactured by cutting pre-confectioned PMMA sheets with a CO_2 laser cutting system (Epilog, Golden, Colorado USA). Micro-channels for fluidic connections, mixer, and gas exchange were fabricated on 500 μm PMMA by scoring the surface applying very low power and speed settings of 3 W and 16 cm/s, respectively, resulting in channels of approximately triangular cross section and about 100 μm depth.

The sample chamber was cut through the same PMMA sheet using higher power and speed settings of 9 W and 26 cm/s, respectively. Top and bottom cover layers were cut from 200 μm PMMA using power and speed settings of 6 W and 26 cm/s, respectively. At the final stage, the top cover layer were further exposed to the laser at 3 W and 16 cm/s for fabricating the fluidic channels on its surface.

The PDMS layer was fabricated using a 10:1 ratio (w/w) of polydimethylsiloxane (PDMS) prepolymer and curing agent. They were thoroughly mixed, degassed under vacuum for 30 mins, poured onto glass petri dishes to a thickness of 1 mm, and cured at 75°C overnight[21]. The PDMS layer has been cut with the desired dimensions using laser cut with power and speed settings of 6 W and 26 cm/s, respectively.

3.3 Bonding protocol

In preparation for bonding, both PMMA and PDMS layers were thoroughly washed in turn with isopropanol (Aldrich), ethanol (Aldrich), and isopropanol again, and dried under a stream of compressed nitrogen. The PMMA layers were thermally bonded, assisted by dibutyl phtalate (DBP) as a plasticiser[22]. The PMMA bonding surfaces were exposed to an oxygen plasma for 45 sec in a plasma etcher operating at 50 W (Diener, Switzerland).

Subsequently, 18μl (i.e. 1.07 $\mu l/cm^{-2}$) of 2.5% (v/v) DBP in isopropanol were coated onto the bonding surfaces of the top and middle layers, as shown in Fig. 3b, followed by drying for 10 min at 65°C, allowing isopropanol to evaporate.

Finally, all three PMMA layers were assembled in an aluminium mould, and exposed to a pressure of 20 MPa at 90°C for 10 min using a laboratory hot plate press (Specac, United Kingdom). The bonded chip was then removed from the aluminium mould and allowed to cool slowly to room temperature.

The bonded PMMA chip and the PDMS layer were cleaned using isopropanol - ethanol - isopropanol and dried with ni-
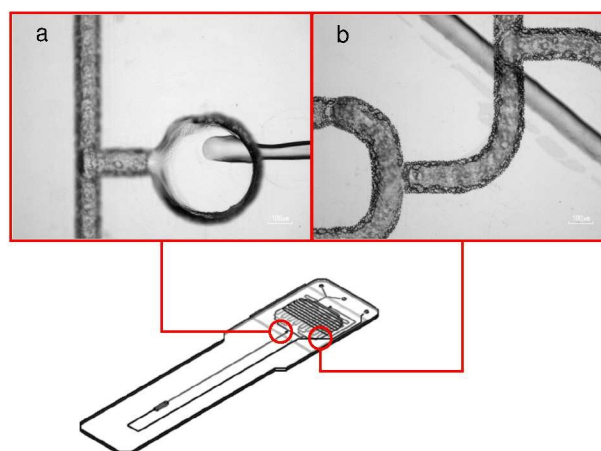

Fig. 4 Micrographs of microfluidic LoC device. a: bright field image showing channels in the gas exchange layer (vertical on the left), a connection via to the middle layer, and a middle layer channel. b: gas exchange channels exhibit a rough surface as a result of fabrication, while the roughness has been eliminated as a side-effect of DBP-assisted bonding.

trogen gas. PDMS/PMMA bonding was carried out following a procedure described by Tang and Lee[23]. The PDMS and PMMA bonding surfaces were treated with oxygen plasma at 50 W for 40 s. The PDMS layer was then dipped into 5% (v/v) aqueous solutions of 3-aminopropile triexhoxylane (APTES), and the PMMA chip was dipped in 3-glycidoxypropyl triethoxysilane (GPTES). The layers were left in contact with the APTES and GPTES solutions at 65°C for 50 min before being thoroughly washed and dried. The bonding surfaces were then carefully joined, and the resulting hybrid chips were annealed for 4 h at 80°C.

Finally, the devices were flushed with clean isopropanol twice, and left to dry at 60°C for at least 24h.

3.4 Glucose oxidation experiments

Glucose oxidation experiments using the chip shown in Fig. 1 were carried out using a solution of 100 mM glucose in 200 mM sodium acetate (NaAc) buffer at pH 5.5 (Solution A), and an enzyme solution (Solution B) containing 31.5 μM glucose oxidase (10 u in 10 μL) and 16 μM catalase (0.8 u in 10 μL), in 200 mM NaAc buffer at pH 5.5. 20 mM 4,4-dimethyl-4-silapentane-1-sulfonic acid (DSS) were added to both solutions as an NMR chemical shift reference.

Solutions A and B were filtered through a 1 μm polycarbonate filter, and then filled into two separate syringe pumps (LabSmith Co., Livermore, CA, US). Each syringe pump was connected to one of the entrance ports in the microfluidic chip using approximately 20 cm of PEEK tubing of 100 μm inner diameter.

Solutions A and B were injected into the chip simultaneously at flow rates q and $0.1q$, respectively. In each experiment, the total volume injected was more than 5 times the chip sample volume, to ensure steady-state conditions. The chip
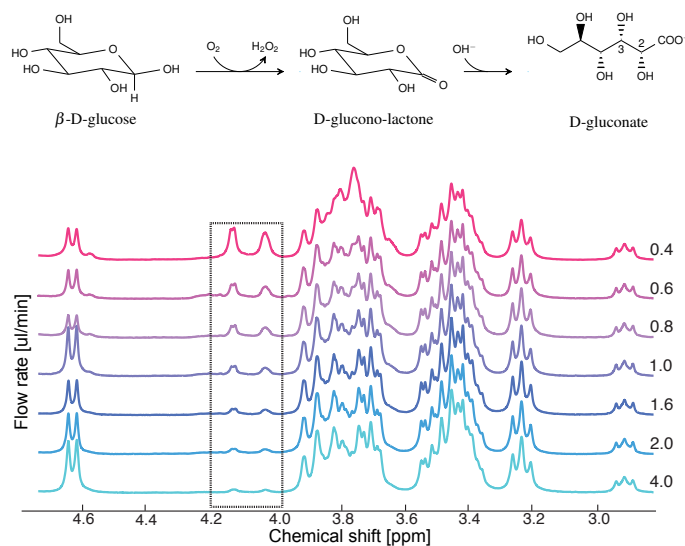
Fig. 5 Observed ^{1}H NMR spectra as a function of flow rate. The area where peaks associated with gluconate appear is indicated.

was then disconnected from the syringe pumps, and the ports were immediately sealed. The concentration of gluconate was then determined by NMR as described below.

3.5 NMR

[1] H NMR data were recorded on a Bruker Avance III 300 MHz spectrometer equipped with a 7 T Oxford magnet, using a special transmission line NMR probe based on the detector design shown in Fig. 1B[1]. Spectra were obtained with solvent presaturation and a 128 ms T_2 filter consisting of a spin echo train with suppressed J evolution[24]. For each analysis, 256 transients were collected as 64k data points with a spectral with of 5000 Hz and inter-pulse delay of 3s between each transient. The total time for each NMR measurement was 27 min. All NMR data was processed using in-house routine in Mathematica. The free induction decay signal was zero filled to 128k points before Fourier transformation, and 0.3 Hz of line broadening was applied. Finally, the gluconate concentrations were determined by integrating the peaks at 4.05 ppm and 4.15 ppm, which correspond to protons at positions 3 and 2, respectively (cf Fig. 5).

4 RESULTS AND DISCUSSION

4.1 Chip quality

The bonding protocol described in the experimental section was the result of a significant optimisation effort. A variety of techniques have been developed for bonding homogeneous or heterogeneous polymer pairings by exposing them to heat[25,26], microwaves[27], or solvents[28,29]. Other approaches have used glue[30], or in situ polymerisation[31] for bonding.

Several of these techniques have been tried in the course of this work, but were found to be unsuitable, producing ei-

ther uneven bonds, or leading to buckling and warping of the microfluidic LoC device. Integration of the LoC device with the NMR detector requires a small overall thickness (less than 1 mm), which makes the structure prone to buckling induced by solvent swelling. While minor buckling may not be a problem in other applications, the homogeneity of the magnetic field depends on the planarity of the LoC device, and intolerable line broadening was observed as a result of poor control of the out-of-plane chip geometry. Our experiments showed that even a state-of-the art solvent vapour approach[32] for bonding PMMA, which has been shown to produce excellent results using thicker material, was unsuitable in the present context for this reason.

Instead, we employed a plasticiser-assisted bonding approach[22], which relies on coating the PMMA surface with dibutyl phtalate (DBP), and subsequent bonding under pressure and somewhat elevated temperature. After careful optimisation of the amount of DBP/isopropanol solution applied to the surface, devices with good planarity could be produced with high yield.

Microfluidic structures were fabricated using a laser cutter. Using a low power setting produced channels of about 100 μm width and similar depth. The surface of these channels was quite rough, as can be seen in Fig. 4a and b. However, the exposure to the plasticiser and isopropanol solvent led to smoothing of the channels, which is clearly visible in the figure. The channels exhibiting rough surfaces are part of the gas exchanger, which was not exposed to the plasticiser during bonding. By contrast, channels in the middle layer (the one leaving the via towards the right in Fig. 4a and the diagonal one from the top to the right of Fig. 4b) do not show any apparent roughness after bonding.

4.2 Oxygen Uptake

Fig. 5 shows ^{1}H NMR spectra as a function of injection flow rate. Peaks due to glucose appear between 4.0 ppm and 3.2 ppm, as well as at 4.65 ppm. The small triplet at 2.9 ppm is due to the DSS standard. The concentration of D-gluconate can conveniently be inferred from the two peaks at 4.17 ppm and 4.02 ppm, which are due to the protons at positions 2 and 3 in D-gluconate, respectively. As expected, and as clearly visible in the figure, the gluconate concentration rises monotonously as the flow rate into the chip decreases.

Glucose oxidase catalyses the reaction shown in Fig. 5, using one half of an oxygen molecule to produce one molecule of gluconate. The hydrogen peroxide that is also produced is reconverted to molecular oxygen by peroxidase. This means that the final amount of of gluconate corresponds to twice the amount of molecular oxygen that has been taken up by the solution.

The resulting gluconate concentrations are shown in Fig. 6 as a function of injection flow rate. Three data sets, obtained on three different days from separately prepared solutions, are shown by blue, orange, and green circles. With the exception of two outliers, the data are remarkably consistent. It should be noted that no attempt to stabilise the experimental temper-
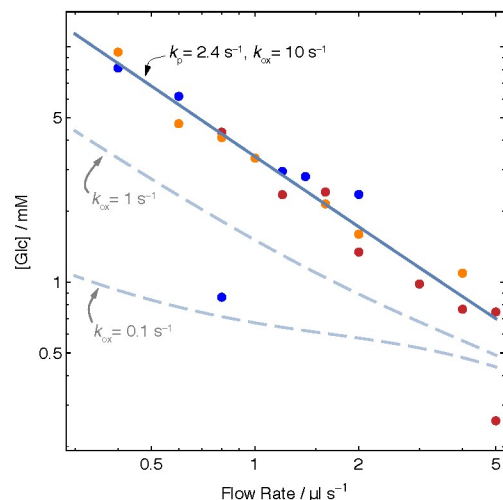
Lab on a Chip Accepted Manuscript

Fig. 6 Measured (solid dots) and predicted (solid line) concentrations of gluconate as a function of flow rate. The experiment was run in a regime of $k_{ox} \gg k_p$. The dashed lines show model predictions for lower values of k_{ox}.

ature has been made beyond the air conditioning system in the laboratory, and small temperature variations probably account for a significant part of the remaining data scatter.

The gluconate concentration was found to be inversely proportional to the flow rate over the entire data range of slightly more than an order of magnitude. The data are in good agreement with the prediction of eq. (7) for a permeation rate constant of $k_p = 2.4\ \mathrm{s}^{-1}$. The exact value of the apparent oxidation rate constant k_{ox} does not significantly affect the quality of the fit, as long as it is larger than $10\ \mathrm{s}^{-1}$; predicted curves for lower values of k_{ox} are shown as dashed lines in the figure for comparison. Clearly, the experimental conditions correspond to a regime where $k_{ox} \gg k_p$.

These findings have important implications for the future use of devices derived from the present one for perfusion culture. The growth medium will be circulated in a closed cycle between the gas exchanger and the sample chamber containing the growing cells. Under these conditions, oxygen is consumed by the cells in the sample chamber, rather than directly in the oxygen exchanger as in the current experimental setup. It is easily shown that the concentration of oxygen in the fluid exiting from a gas exchanger of length L is given by

$$c_{out} = (c_{in} - c_{eq})e^{-\frac{k_p whL}{q}} + c_{eq}, \qquad (9)$$

where c_{in} is the oxygen concentration at the entrance to the gas exchanger, q is the flow rate, and w and h denote the width and height of the gas exchange channel, respectively. Note that $whL/q = \tau$, where τ is the residence time of the fluid in the gas exchanger. In a stationary state, the difference between c_{in} and c_{out} compensates the rate of oxygen consumption of the cells R:

$$R = q(c_{out} - c_{in}) = q\,\Delta c\left(1 - e^{-\frac{k_p whL}{q}}\right), \qquad (10)$$

where $\Delta c = c_{eq} - c_{in}$ is the difference between the equilibrium oxygen concentration and that of the fluid entering the gas exchanger. The rate of oxygen consumption varies considerably with cell type, and tends to be relatively high in cancer cell lines. As an example, we consider the value for human mammary adenocarcinoma cells (MCF-7), which has been given[33] as $50 \times 10^{-18}\ \mathrm{Mol\,s^{-1}\,cell^{-1}}$. If we assume a cell culture containing 10^4 cells, (10) predicts that flow rate of no less than $0.02\ \mu\mathrm{l\,s^{-1}}$, or about $1\ \mu\mathrm{l\,min^{-1}}$, will be sufficient to restrict the drop in oxygen concentration to $\Delta c < 10\,\mu\mathrm{M}$, or 5% of the equilibrium value.

It should be noted that the current device is made from PMMA. While PMMA is often used as a biocompatible material in implants and bone cements etc, it has been shown that it is less than ideal as a substrate for the culture of adherent mammalian cells[34]. Other glassy polymers, in particular poly(styrene) (PS) are more commonly used for this purpose. While we have preliminary data indicating that MCF-7 cells grow as well on our substrate as on standard PS well plates, this is a point that requires further investigation as the present platform is developed. However, all of the fabrication and bonding protocols used can be applied just as well to PS as to PMMA, and therefore substitution of the chip material, at the very least for the base layer, should be straightforward. Also, various techniques for surface modification and coating of PMMA are available.

Finally, cell culture requires not only oxygen access, but also exchange of CO_2 with the atmosphere to ensure a stable pH in the culture medium. As the permeability of PDMS for CO_2 is known to be more than 5 times greater than for O_2,[6] this should not pose any problem for the device presented here.

5 CONCLUSIONS

We report a microfluidic LoC device that is capable of maintaining normoxic conditions in perfusion culture of mammalian cells, while at the same time being compatible with in-situ observation by high-sensitivity, high resolution micro-NMR spectroscopy. While the permeability for molecular oxygen and other gases of PDMS is commonly exploited in microfluidic cell culture devices, a major challenge arises due to the incompatibility of PDMS with NMR spectroscopy. We have circumvented this by separating the gas exchange through a PDMS membrane from the sample chamber in a chip made from PMMA. A fabrication protocol using inexpensive laser cutting from commercial sheet material in conjunction with plasticiser-assisted bonding has been optimised for the base chip, and the PDMS gas exchange membrane has been bonded by silane/epoxide surface chemistry.

The oxygen permeation has been quantified by injecting solutions of glucose and glucose oxidase/hydrogen peroxidase into the device at defined flow rates. The total oxygen uptake could then be determined through the concentration of gluconate formed, which was measured by in-situ NMR spectroscopy. At the same time, these experiments have confirmed the compatibility of the device with high-resolution micro

NMR spectroscopy.

It was found that the rate constant for oxygen permeation in this device is $k_p = 2.4\,\mathrm{s}^{-1}$, meaning that equilibration with the outside oxygen partial pressure can be achieved in an exposure time of the order of $1/k_p = 0.42$ s. It is shown that the device is capable of supplying enough oxygen to maintain normoxic conditions in a perfusion cell culture containing up to 10'000 MCF-7 cells.

The new device opens the possibility to study cell metabolism under normoxic conditions in a close-cycle perfusion platform by non-invasive NMR spectroscopy. Experiments along these lines are currently underway in our laboratory; the results will be reported at a later occasion.

Acknowledgements

References

1 G. Finch, A. Yilmaz and M. Utz, *Journal of Magnetic Resonance*, 2016, **262**, 73–80.

2 J. El-Ali, P. K. Sorger and K. F. Jensen, *Nature*, 2006, **442**, 403–411.

3 P. M. van Midwoud, M. T. Merema, E. Verpoorte and G. M. M. Groothuis, *Lab Chip*, 2010, **10**, 2778.

4 A. Khademhosseini, R. Langer, J. Borenstein and J. P. Vacanti, *Proceedings of the National Academy of Sciences*, 2006, **103**, 2480–2487.

5 Q. Liu, C. Wu, H. Cai, N. Hu, J. Zhou and P. Wang, *Chemical Reviews*, 2014, **114**, 6423–6461.

6 W. L. Robb, *Annals of the New York Academy of Sciences*, 1968, **146**, 119–137.

7 J. Nicholson, E. HOLMES and J. Lindon, *The Handbook of Metabonomics and Metabolomics*, 2007, 1.

8 C. Massin, G. Boero, F. Vincent, J. Abenhaim, P. Besse and R. Popovic, *Sensors & Actuators: A. Physical*, 2002, **97**, 280–288.

9 E. McDonnell, S. Han, C. Hilty, K. Pierce and A. Pines, *Anal. Chem*, 2005, **77**, 8109–8114.

10 Y. Maguire, I. Chuang, S. Zhang and N. Gershenfeld, *Proc. Natl. Acad. Sci. USA*, 2007, **104**, 9198–9203.

11 A. P. M. Kentgens, J. Bart, P. J. M. van Bentum, A. Brinkmann, E. van Eck, J. G. E. Gardeniers, J. W. G. Janssen, P. Knijn, S. Vasa and M. H. W. Verkuijlen, *J Chem Phys*, 2008, **128**, 052202.

12 M. Utz and R. Monazami, *Journal of Magnetic Resonance*, 2009, **198**, 132–136.

13 H. Ryan, S.-H. Song, A. Zaß, J. Korvink and M. Utz, *Anal. Chem*, 2012, **84**, 3696–3702.

14 V. Badilita, R. C. Meier, N. Spengler, U. Wallrabe and M. Utz, *Soft Matter*, 2012.

15 N. Spengler, A. Moazenzadeh, R. C. Meier, V. Badilita, J. G. Korvink and U. Wallrabe, *J. Micromech. Microeng.*, 2014, **24**, 034004.

16 S. S. Zalesskiy, E. Danieli, B. Blümich and V. P. Ananikov, *Chem. Rev*, 2014, **114**, 5641–5694.

17 A. Smith, c. vallance, G. Finch and M. Utz, Experimental Nuclear Magnetic Resonance Conference, Boston, 2014.

18 A. Kalfe, A. Telfah, J. Lambert and R. Hergenröder, *Analytical chemistry*, 2015, **87**, 7402–7410.

19 N. Spengler, J. Höfflin, A. Moazenzadeh, D. Mager, N. MacKinnon, V. Badilita, U. Wallrabe and J. G. Korvink, *Plos One*, 2016, **11**, e0146384.

20 D. Tromans, *Hydrometallurgy*, 1998, **48**, 327–342.

21 D. C. Duffy, J. C. McDonald, O. Schueller and G. Whitesides, *Analytical chemistry*, 1998, **70**, 4974–4984.

22 H. Duan, L. Zhang and G. Chen, *Journal of Chromatography A*, 2010, **1217**, 160–166.

23 L. Tang and N. Y. Lee, *Lab Chip*, 2010, **10**, 1274–1280.

24 J. A. Aguilar, M. Nilsson, G. Bodenhausen and G. A. Morris, *Chem. Commun.*, 2012, **48**, 811–813.

25 C. L. do Lago, H. da Silva, C. A. Neves, J. Brito-Neto and J. da Silva, *Analytical chemistry*, 2003, **75**, 3853–3858.

26 Y. Sun, Y. C. Kwok and N.-T. Nguyen, *J. Micromech. Microeng.*, 2006, **16**, 1681–1688.

27 A. A. Yussuf, I. Sbarski, J. P. Hayes, M. Solomon and N. Tran, *J. Micromech. Microeng.*, 2005, **15**, 1692–1699.

28 L. Brown, T. Koerner, J. H. Horton and R. D. Oleschuk, *Lab Chip*, 2006, **6**, 66–73.

29 X. Sun, B. A. Peeni, W. Yang, H. A. Becerril and A. T. Woolley, *Journal of Chromatography A*, 2007, **1162**, 162–166.

30 L. G. Song, D. F. Fang, R. K. Kobos, S. J. Pace and B. Chu, *Electrophoresis*, 1999, **20**, 2847–2855.

31 G. Chen, J. Li, S. Qu, D. Chen and P. Yang, *Journal of Chromatography A*, 2005, **1094**, 138–147.

32 I. R. G. Ogilvie, V. J. Sieben, C. F. A. Floquet, R. Zmijan, M. C. Mowlem and H. Morgan, *J. Micromech. Microeng.*, 2010, **20**, 065016.

33 B. A. Wagner, S. Venkataraman and G. R. Buettner, *Free Radical Biology and Medicine*, 2011, **51**, 700–712.

34 P. M. van Midwoud, A. Janse, M. T. Merema, G. M. M. Groothuis and E. Verpoorte, *Anal. Chem*, 2012, **84**, 3938–3944.